Journal of Molecular Graphics and Modelling 39 (2013) 71–78

Contents lists available at SciVerse ScienceDirect

Journal of Molecular Graphics and Modelling

journal homepage: www.elsevier.com/locate/JMGM

Association of nicotinic acid with a poly(amidoamine) dendrimer studied by molecular dynamics simulations

Julio Caballero*, Horacio Poblete, Cristell Navarro, Jans H. Alzate-Morales

Centro de Bioinformática y Simulación Molecular, Universidad de Talca, 2 Norte 685, Casilla 721, Talca, Chile

ARTICLE INFO

Article history:
Accepted 8 November 2012
Available online 19 November 2012

Keywords:
PAMAM
Nicotinic acid
Molecular dynamics
Dendrimer

ABSTRACT

The interaction of poly(amidoamine)-G3 (PAMAM-G3) dendrimer with nicotinic acid (NA) was investigated by using molecular dynamics (MD) simulations. First, sample free energy profiles of NA crossing PAMAM-G3 at pH 6 and 3 were computed using the adaptive biasing force (ABF) method. We found that PAMAM-G3 provides a more appropriate environment for NA inclusion when internal tertiary amine groups are unprotonated (at pH 6). However, when internal tertiary amine groups are protonated (at pH 3), the PAMAM cavities are less hydrophobic; therefore the drug–dendrimer interactions become similar to drug–solvent interactions. Traditional MD simulations were also performed to investigate the structural stability of the PAMAM–NA complexes near the free energy minima at pH 6. We found that association of NA and PAMAM adopts a preferred binding mode around the surface of PAMAM, where hydrogen bond (HB) interactions with the amino and amide NH groups of the nearby monomers are established. These interactions are very stable whether additional van der Waals interactions between pyridine ring of NA and methylene groups of the more external monomers of PAMAM are established.

1. Introduction

In recent years, supramolecular chemistry has become a very important area where noncovalent interactions between molecules have been intelligently used [1]. In nanoscience, complexes systems such as biomacromolecule–metal nanoparticles aggregates [2], biomacromolecule–carbon nanotubes assemblies [3], dendrimer–drug and dendrimer–biomacromolecule complexes [4,5], etc., have emerged as promising devices with potential applications in medicinal chemistry. The formation of these supramolecular complexes occurs through a multiplicity of often difficult to differentiate noncovalent forces. The structural characterization of these highly complex structures and their interaction mechanisms are ongoing challenges.

Dendrimers, spherical and mono-disperse polymers with a tree-like or generational structure, have generated a tremendous interest for many applications ranging from materials science to biomedical applications [6–8]. Dendrimers have internal cavities and functional end groups which can interact with small molecules increasing their solubilities. Due to this, dendrimers are versatile platforms in drug delivery applications [4]. Polyamidoamine (PAMAM) dendrimers and their derivatives are the most studied starburst macromolecules [9,10]. PAMAM dendrimers have much higher amino group densities comparing with conventional macromolecules; they have several internal tertiary amine groups, amide groups, and primary amine terminal groups. Accordingly, structure and chemical properties of PAMAM dendrimers are highly dependent on pH, which is a critical issue for utilization as drug delivery vehicles in physiological environments [11].

Drugs or small molecules can either be attached to PAMAM end groups or encapsulated in the macromolecule interior [12–15]. Nicotinic acid (NA), known as vitamin B_3 or niacin, is essential for cell respiration, metabolism of carbohydrates, fats and proteins, healthy skin and circulation, etc. Furthermore, it has been reported that NA prevents Alzheimer's-like symptoms [16], and it is used in the treatment of schizophrenia and other mental illnesses [17]. Despite its multiple roles, NA is not soluble in water at room temperature. With this in mind, Yiyun and Tongwen recently used PAMAM dendrimers to increase the solubility of NA [12]. They found that PAMAM dendrimers have the potential to significantly enhance the solubility of NA, and the drug solubility depends on the concentration of the dendrimer, the pH value of the solution, and surface functional group and the generation of the dendrimer. Regarding the pH conditions, dendrimers cause the higher increase in NA solubility at higher pH values. Authors suggest that this behavior is due to that NA, being weakly acid, is not fully ionized at low pH conditions and hence cannot freely interact electrostatically with the surface amine groups of dendrimer molecule. However, considering that pKa of the aromatic ring nitrogen is 4.9 and pKa of the COOH group is 2.18 for NA [18], then the NA exists as

* Corresponding author. Tel.: +56 71 201 685; fax: +56 71 201 662.
E-mail addresses: jcaballero@utalca.cl, jmcr77@yahoo.com (J. Caballero).

1093-3263/$ – see front matter © 2012 Elsevier Inc. All rights reserved.
http://dx.doi.org/10.1016/j.jmgm.2012.11.003

3-pyridiniumcarboxylate at pHs 3 and 4 since both groups should be ionized (NA exists as nicotinate at pH 6). In this sense, the electrostatic interactions should increase at these pHs. Authors also justified the above mentioned effect by considering that the cavity environment inside the PAMAM dendrimer at pH 6 is more hydrophobic than that of the aqueous phase outside. At low pH conditions, protonation of the tertiary amines in the full generation dendrimers enhances the polar level of environment inside the dendrimer, which causes no significant increase in the solubility of NA.

In the current report, we studied the interactions between NA and PAMAM-G3 by using molecular dynamics (MD) simulations in aqueous solution. First, the interactions with dendrimer models representing pHs 3 and 6 states were examined by using the adaptive biasing force (ABF) method [19,20]. The free energy profiles along a prescribed path (a reaction coordinate) delineating the movement of the 3-pyridiniumcarboxylate or nicotinate across PAMAM-G3 were compared for these models. In addition, some stationary points found on the free energy landscape were further examined by means of additional MD simulations at pH 6, where interactions are higher. The analysis of the MD trajectories allows describing the structural features of the complex at the molecular level.

2. Methods

2.1. Molecular structures and parameters

Models of PAMAM dendrimers of generations 3–6 were built for testing the developed CHARMM parameters for PAMAM. In addition, two PAMAM-G3 models were used for studying interactions between NA and PAMAM at different pHs. PAMAM dendrimers containing a 1,2-ethanediamine core and the surface amine groups protonated were built using the program Hyperchem [21]. The dendrimers were built by increasing their size from the core to generations 3, 4, 5 and 6 respectively; in each step of increase, the models were optimized by using AM1 semiempirical method [22]. The models of nicotinate and 3-pyridiniumcarboxylate were also built using the program Hyperchem [21].

All the molecules were parameterized according to the rules for all-atom CHARMM27 force field [23]. Charges, missing bond, angle, and dihedral parameters of PAMAM core and monomers were estimated from similar terms within the force field. Charges and parameters for nicotinate were derived from parameters developed for Yin for pyridines [24], and those for 3-pyridiniumcarboxylate were obtained using the program Paratool implemented in VMD (Visual molecular dynamics) [25]. Paratool generates input files for programs of quantum mechanics (QM) calculations (Gaussian in our work). This program reads and extracts, from the output files of QM, dihedral parameters of connection, angles, improper angles, partial charges and it transforms the hessians of quantum mechanics into numerical values with units in kcal/mol, Angstrom and degrees, besides writing the internal coordinates of the molecule. Also it can assign to the type of atom and its radius of van der Waals (VdW) corresponding for existing atoms in the force fields. Finally it collects all these data and writes archives of topology and parameters for molecules that are necessary to accomplish MD calculations.

2.2. Molecular models

The microscopic charging mechanism of dendrimers is not immediately obvious and has prompted quite some discussion in the literature [26]. In this work we constructed two ideal models to represent PAMAM-G3 systems at pH 6 and 3. The model at pH 6 included the PAMAM-G3 with surface amine groups protonated and the nicotinate. The model at pH3 included the PAMAM-G3 with internal tertiary amine and surface amine groups protonated, and the 3-pyridiniumcarboxylate. For both models, the PAMAM-G3 dendrimers were aligned with the z axis, and the center of mass of them were set to the origin of the coordinate system. For hydration of each model, a water box confined by a periodic boundary condition was added to the simulation system, and then the system was neutralized. The initial size of the water box was $87.4 \times 88.6 \times 112.4\,\text{Å}^3$ for the model at pH 6, and $87.3 \times 88.4 \times 112.4\,\text{Å}^3$ for the model at pH 3, involving 25,818 and 27,063 water molecules, respectively. To neutralize the system, 31 and 62 chloride ions, respectively, were added. These models are represented in Fig. 1.

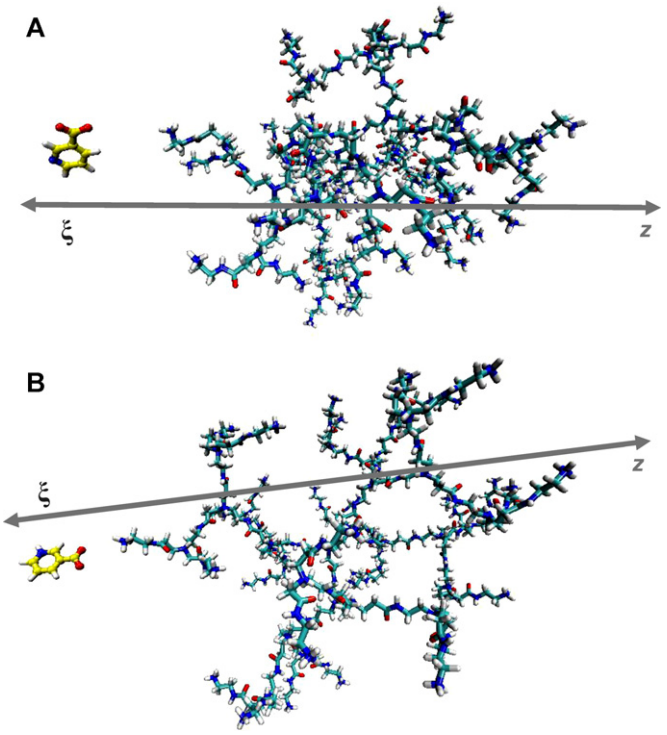

Fig. 1. Scatter schematic representation of the models: (A) at pH 6 and (B) at pH 3. The paths (ξ) delineating the movement of the nicotinate and 3-pyridiniumcarboxylate across PAMAM-G3 were indicated. Water box and ions were omitted for clarity.

2.3. Molecular dynamics simulations

The models were energy-minimized by conjugate gradient method for 1000 steps, and then, they were subjected to 2.0 ns of equilibration. All MD simulations were carried out using the program NAMD [27], CHARMM force field [23], and the TIP3P water model was used [28]. The equations of motion were integrated with a 1-fs time step. The lengths of those covalent bonds between heavy and hydrogen atoms were frozen to their equilibrium value. The VdW cutoff was set to 12 Å. The temperature was maintained at 310 K, employing Langevin dynamics with a damping coefficient of $1\,\text{ps}^{-1}$. The Nosé-Hoover Langevin piston was used to control the pressure at 1 atm, with a piston period of 100 fs, a damping time constant of 50 fs, and a piston temperature of 310 K. Long-range electrostatic forces were taken into account by means of the particle-mesh Ewald approach. The present calculations were carried out on a HP Blade bl640c (Xeon5420 based) Cluster with a Infiniband 4xDDR switch.

The study of the interactions between NA and PAMAM-G3 using MD simulations were developed in two stages. First, sampled free energy profiles describing the movement of NA inside PAMAM-G3 systems at pH 6 and 3 were built using adaptive biasing force (ABF) method. After this, traditional MD simulations were developed using structures of the complex at pH 6 as starting points. These structures correspond to minima of the free energy profile derived using ABF.

2.3.1. Adaptive biasing force (ABF) calculations

The free energy along an appropriate ordering parameter, ξ, describing the movement of the nicotinate or 3-pyridiniumcarboxylate through a sample path inside PAMAM-G3, was estimated using the ABF method in which a biasing force is rapidly estimated and refined to erase the ruggedness of the free energy surface, and, hence, allow ξ to be sampled uniformly. Next, the free energy is determined by integrating the average force acting along ξ, obtained from unconstrained MD simulations [19,20]. Prior to each ABF run, the molecular assemblies formed by the PAMAM, nicotinate or 3-pyridiniumcarboxylate, ions and their aqueous medium were equilibrated over a period of 500 ps. The ABF coordinate was zCoord for all the ABF calculations. When running the free energy calculations, the oxygen atoms of two water molecules near the (0, 0, z) vector and located to both sides of PAMAM molecule were fixed, and center of mass of nicotinate (or 3-pyridiniumcarboxylate) was constrained on the z axis to make sure the drug moved along the selected sample direction.

It is important to note that a sample trajectory was selected for applying ABF method with the aim of comparison between the two systems at pH 6 and 3. Many other trajectories could have been selected and other free energy profiles could have been derived. However, one sample profile is enough to compare the complexes.

Since the path along the z axis is not a cavity, the drug was not constrained on the xy-plane; therefore, the molecule can move around that plane when it finds a physical barrier in its way. For all systems, convergence was probed by extending the total simulation time and assessing the evolution of the average force as a function of time. The pathway, between −46 and 46 Å in z-axis, was divided into 23 consecutive windows to further increase the efficiency of the calculations. 2.5 ns simulations were carried out in each window, where the instantaneous values of the force acting along the ordering parameter ξ were accrued in small bins of width $\delta\xi$ = 0.1 Å, accumulating N_{samples} = 1000, prior to application of the adaptive bias. The average force was interpolated over the adjacent bins and progressively applied along ξ by means of a linear ramp.

2.3.2. Traditional MD calculations

We selected the structures of the complex at pH 6 that correspond to minima of the free energy profile obtained by ABF calculations to investigate the stability of the interactions between the NA and PAMAM-G3 at these conformations. For this, we performed traditional 5-ns MD simulations using the conditions described above in Section 2.3.

3. Results and discussion

The new CHARMM parameters developed for PAMAM were tested. We carried out 5-ns MD simulations of different PAMAM of generations 3–6 in water, and measured mean-square radius of gyrations (R_{GYR}) of the dendrimers from the last 3 ns of each simulation. PAMAM dendrimers were prepared as described in Methods section for PAMAM-G3 at pH 6 (only the surface amine groups protonated). Recent experiments showed that R_{GYR} values of PAMAM dendrimers are essentially independent of pH [29]; in this sense, we can compare our calculated R_{GYR} values with other reported R_{GYR} values at different pHs. Each water box had periodic boundary condition and each system was neutralized. The number of atoms, ions and the initial size of the water box for each simulation are indicated in Table 1.

Table 1
Number of atoms, terminal nitrogen (or chloride ions), water molecules, and size of water box for fully atomistic models of PAMAM dendrimer for G3 to G6.

Generation	No. of terminal nitrogens or chloride ions	No. of atoms	No. of water molecules	Size of water box (Å^3)
3	32	64,549	21,131	88 × 88 × 88
4	64	113,627	37,085	106 × 106 × 106
5	128	182,044	59,080	124 × 124 × 124
6	256	207,584	65,972	130 × 130 × 130

For a dendrimer with N atoms the mean-square R_{GYR} is given by

$$\langle R_{GYR}^2 \rangle = \left(\frac{1}{M}\right) \left\langle \left[\sum_{i=1}^{N} m_i |r_i - R|^2 \right] \right\rangle \quad (1)$$

where R is the center of mass of the dendrimer, m_i is the mass of the ith atom, r_i is the relative position of the ith atom with respect to R, and M is the total mass of the dendrimer. Table 2 shows the R_{GYR} as a function of generation. We see good agreement between our calculated R_{GYR} with those obtained from small-angle neutron scattering (SANS) [30] and small-angle X-ray scattering (SAXS) experiments [31]. Table 2 also shows that the R_{GYR} values from our simulations are much closer to experimental R_{GYR} values with respect to previous simulations performed with Dreiding force field in a vacuum [32], and with Amber force field with explicit solvent and counterions [33–35]. Our R_{GYR} value for PAMAM-G4 was comparable to the recently obtained by Liu et al. [29] from MD simulations with explicit solvent and counterions using a Dreiding force field whose intermolecular parameters were optimized using quantum mechanics.

The free energy profiles characterizing the advance of NA into PAMAM-G3 at pHs 3 and 6 are depicted in Fig. 2. No significant differences were observed when simulations were extended from 57.5 to 69 ns; in this sense, it would appear that 57.5 ns are enough to obtain a reasonably converged PMF. It could be noticed that, qualitatively, the free energy profiles are quite different: the free energy profile characterizing the advance of nicotinate into PAMAM-G3 at pH 6 has several local minima with free energies among −1.5 and −3 kcal, while the free energy profile characterizing the advance of 3-pyridiniumcarboxylate into PAMAM-G3 at pH 3 has very small minima with free energies of approximately −0.5 kcal. By comparing these profiles, we can conclude that NA interacts better with PAMAM-G3 at higher pHs, which coincides with previous experimental results [12]. The differences between the profiles indicate that PAMAM-G3 with internal tertiary amine groups unprotonated (at pH 6) provides a more appropriate environment for NA inclusion. However, when internal tertiary amine groups are protonated, the presence of NA inside the PAMAM cavities is less favorable. The free energy profile at pH 3 suggests that drug–dendrimer interactions become similar to drug–solvent interactions at these conditions. This behavior, described by our simulations, is typical of drug-release delivery systems. The interactions of drugs with charged dendrimers are pH-sensitive: the incorporation of the drug is induced in basic environment and its release is favored in acidic media [36].

ABF has been previously used for studying the path of an atom or molecule through pores or cavities located on the z-coordinate [37–40]. In contrast, the path in the current ABF application was determined by the cavities found by the NA molecule inside the dendrimer in its movement in the direction of z-axis with a displacement allowed on xy-planes; in this sense, the obtained

Table 2
Radius of gyration (R_{GYR}) (Å) as a function of generation for PAMAM.

Generation	This work	SAXS[a]	SANS[b]	DFF-MDSiv[c]	DFF-MDSiv[d]	Amber-MD1[e]	Amber-MD2[e]	Amber-MD3[f]
3	15.33 ± 0.30	15.8	16.19	11.23			16.25 (17.96)	
4	21.04 ± 0.41	17.1	20.92	14.50	21.43	20.0 (21.0)	19.00 (21.0)	18.8
5	25.50 ± 0.29	24.1	25.86	18.34		22.9 (24.2)	22.43 (24.23)	
6	30.18 ± 0.23	26.3	31.93	22.40		27.2 (28.9)	27.21 (28.90)	

[a] Small-angle X-ray scattering (SAXS) in CH_3OH [31].
[b] Small-angle neutron scattering (SANS) [30].
[c] Dreiding force field MD simulation in a vacuum [32].
[d] MD simulation with explicit solvent and counterions using a Dreiding force field whose intermolecular parameters were optimized using quantum mechanics [29].
[e] MD simulation with explicit solvent and counterions using a Amber force field at pH 7.4 and pH 5 in parentheses [33,34].
[f] MD simulation with explicit solvent and counterions using a Amber force field at pH 7.4 [35].

paths were samples of the possible pathways of the NA through PAMAM-G3 cavities. Our ABF current study is a bit different with respect to previous studies of the path of atoms or molecules into cavities or pores. We selected an arbitrary starting point for NA around the dendrimer and we could have chosen different directions of penetration than that along *z*-coordinate. We assumed that our selected reaction coordinate represents other possible directions. Since dendrimers are considered spherical molecules, we assumed that the starting position and direction do not play a fundamental role in the obtained free energy profiles.

We observed that the nicotinate inside PAMAM-G3 with internal tertiary amine groups unprotonated (at pH 6) was stabilized by VdW interactions between the aromatic ring of the nicotinate and methylene groups of the last generation of PAMAM-G3 (Fig. 3). It was also stabilized by H-bonds between carboxylate oxygens and pyridinic nitrogen of the nicotinate, and surface amines and amide NH groups of the last generation of PAMAM-G3. In a recent paper, Yang et al. [13] detected that phenylbutazone, a nonsteroidal anti-inflammatory drug, increases its solubility by interacting with the surface of PAMAM-G3 using 2D-NOESY analysis. They found that higher generation PAMAM dendrimers tend to encapsulate more phenylbutazone molecules than lower ones. In fact, they found that a very few phenylbutazone molecules were encapsulated in the cavities of PAMAM-G3; however, the molecules were preferentially encapsulated in PAMAM-G6. This behavior has been justified by the presence of more and larger interior cavities in higher generation dendrimers than in lower generation ones. An interesting point is that dendrimers can lose their host–guest capacity when the generation becomes too large because the dendrimers become so crowded that the access to their interior is prevented to small molecules and also to water [41]. In our current simulations, as mentioned above, we found that nicotinate also prefers to interact with surface groups of PAMAM-G3, instead of to be encapsulated in the macromolecule interior.

Additional 5-ns MD simulations were also performed, using as starting points three structures of the complex at pH 6 that correspond to minima of the free energy profile. Fig. 3 shows the starting nicotinate conformations and the relation of them with their surrounding media. In all the selected starting conformations, nicotinate's carboxylate interacts with a surface amine of PAMAM-G3 (Fig. 3 A–C). However, nicotinate was more exposed to the water in conformation A as can be seen in nicotinate–dendrimer and nicotinate–water radial distribution functions (RDFs) derived from its initial model (Fig. 3D and E). Instead, nicotinate was lesser exposed to the water in conformation B, and it was closer to methylene groups of the last generation of PAMAM-G3 in conformation C (these descriptions also can be derived by analysis of structures and RDFs in Fig. 3B–E).

The 5-ns MD simulations from the above mentioned starting structures were analyzed for explaining the interactions between nicotinate and PAMAM-G3 at a molecular level. For a better understanding, Scheme 1 provides a representation of nicotinate *n* and a PAMAM monomer *m* structures. A scheme of the pathway of nicotinate around PAMAM-G3 surface according to 5-ns MD simulation using conformation A as starting point (MD-A) is represented in Fig. 4A; in addition, Fig. 5 shows distances between some atoms of nicotinate and atoms of PAMAM that the drug found on its way. First, the nicotinate molecule was near the monomer *m*50 of PAMAM-G3 (site I, Fig. 4A). At this site, H-bonds (HBs) between the carboxylate of nicotinate and amine and amide N atoms of *m*50 were formed. This was deduced from the analysis of the distances between carboxylic carbon CD3 of nicotinate and

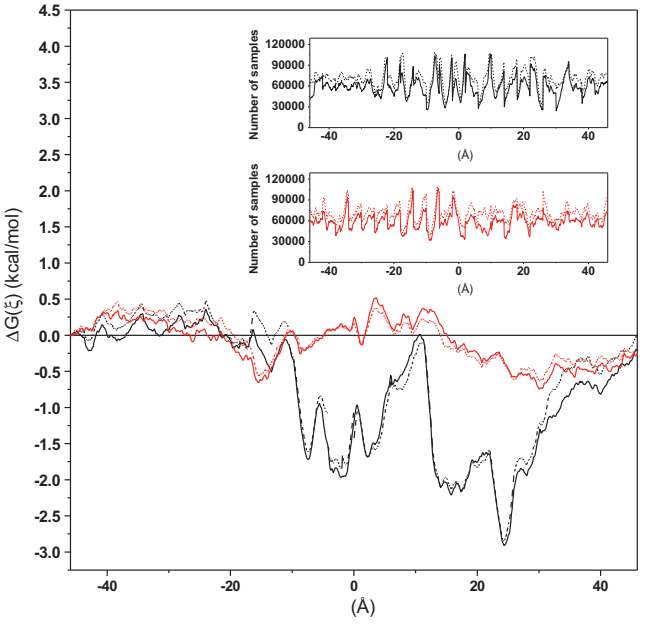

Fig. 2. Free energy profile obtained from ABF calculation for the movement of the nicotinate and 3-pyridiniumcarboxylate across PAMAM-G3. The sampling distribution characteristic of each MD simulation is included in the inset. The free energy profiles for the movement of nicotinate across PAMAM-G3 obtained from 57.5-ns (solid line) and 69-ns (dotted line) simulations are represented in black. The free energy profiles for the movement of 3-pyridiniumcarboxylate across PAMAM-G3 obtained from 57.5-ns (solid line) and 69-ns (dotted line) simulations are represented in red. (For interpretation of the references to color in this figure legend, the reader is referred to the web version of the article.)

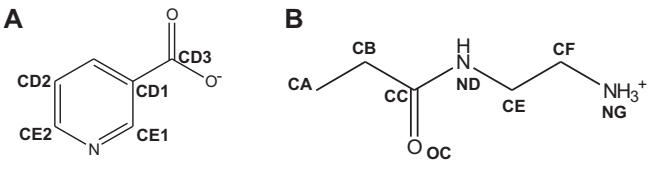

Scheme 1. Structures of (a) nicotinate: *n* and (b) PAMAM end monomer: *m*.

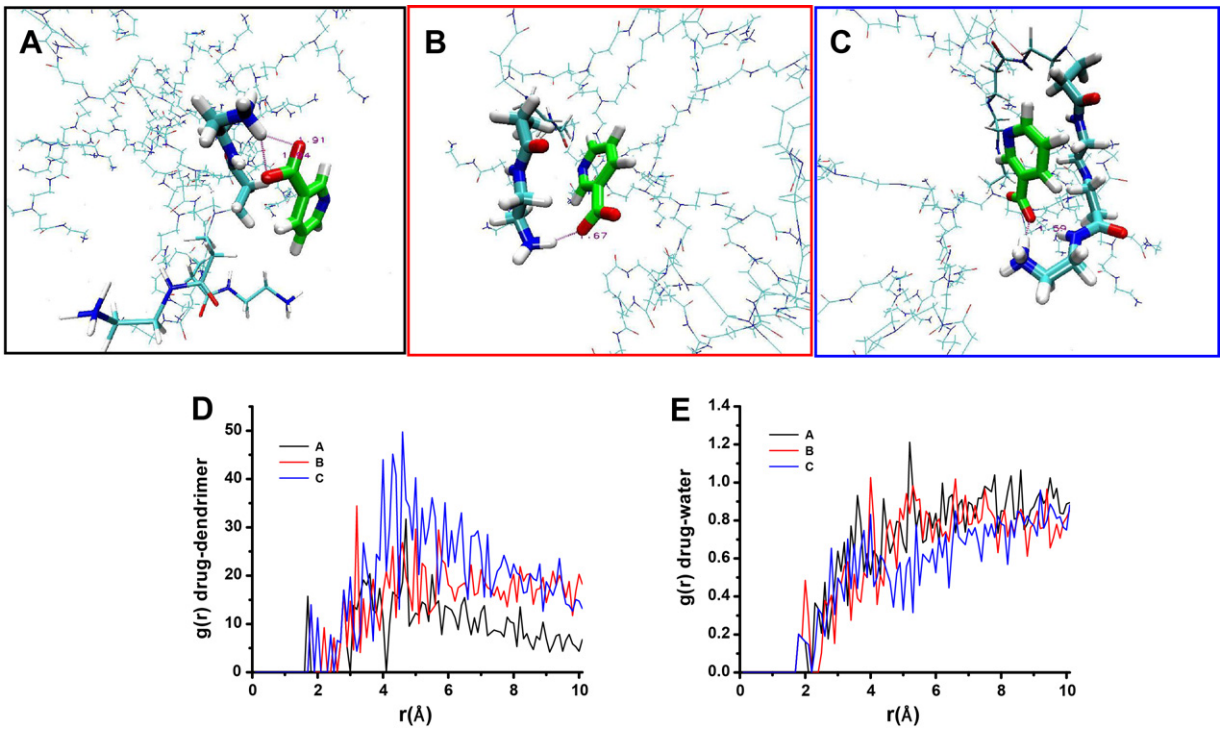

Fig. 3. Snapshots of the nicotinate inside PAMAM-G3 at pH 6 near the free energy minima for starting 5-ns MD simulations: (A) conformation A, (B) conformation B, (C) conformation C, (D) radial distribution function of the dendrimer around the nicotinate for conformations A, B and C, and (E) radial distribution function of the water molecules around the nicotinate for conformations A, B and C.

nitrogen atoms NG and ND of *m*50 (distances CD3(*n*)–NG(*m*50) and CD3(*n*)–ND(*m*50) in Fig. 5): they took values around 3.40 and 3.60 Å respectively from the beginning of the simulation to 1.170 ns. After this time, nicotinate molecule moved away from the surface of PAMAM and entered into the solvent. Nicotinate approximated to the monomer *m*56 of PAMAM-G3 (site II, Fig. 4A) from 2.06 to 2.57 ns. During this time, the distance between carboxylic carbon CD3 of nicotinate and nitrogen NG of *m*56 (distance CD3(*n*)–NG(*m*56) in Fig. 5) was around 3.46 Å due to HB formed between carboxylate of nicotinate and amine N atom of *m*56. After 2.57 ns, the mentioned interaction was broken and nicotinate molecule returned to the solvent. At 3.51 ns simulation time, nicotinate approximated to the monomer *m*57 of PAMAM-G3 (site III, Fig. 4A). At this time, the pyridine ring of nicotinate established VdW interactions with methylene groups of monomers *m*57, *m*27 and *m*28, while the carboxylate group interacted with water molecules. From 3.51 to 4.88 ns, the distance between carbon CD1 of nicotinate and carbon CB of *m*28, the distance between carbon CE2 of nicotinate and carbon CA of *m*27, the distance between carbon CD2 of nicotinate and carbon CE of *m*57, and the distance

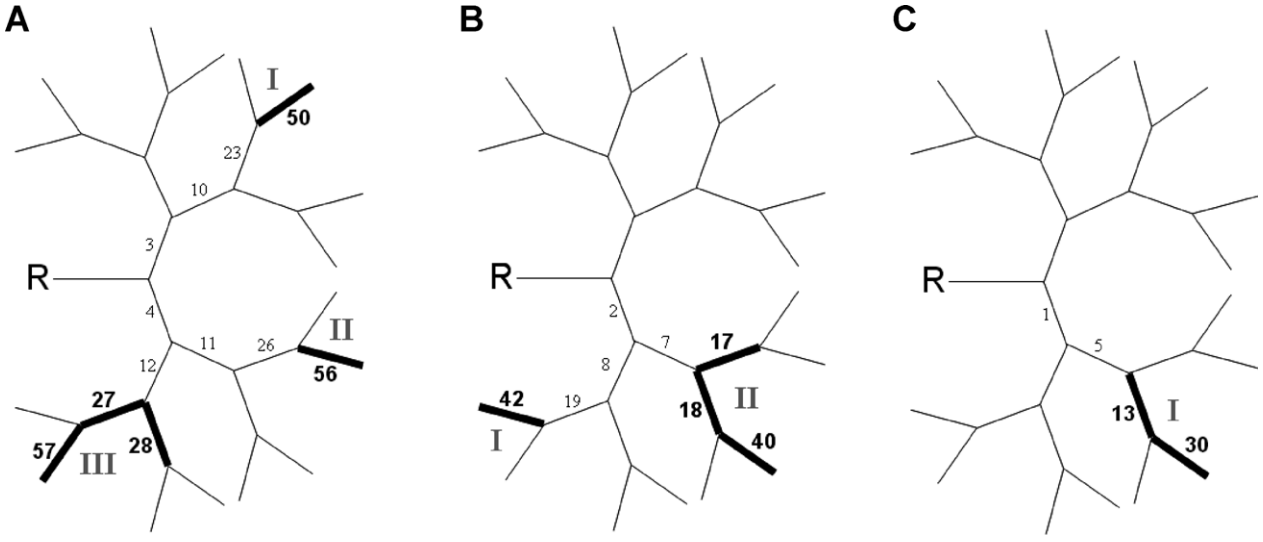

Fig. 4. Schemes of the pathways of nicotinate around PAMAM-G3 surface according to 5-ns MD simulations for (A) conformation A, (B) conformation B, and (C) conformation C. Sites of longer interactions during MD simulations are represented by roman numerals.

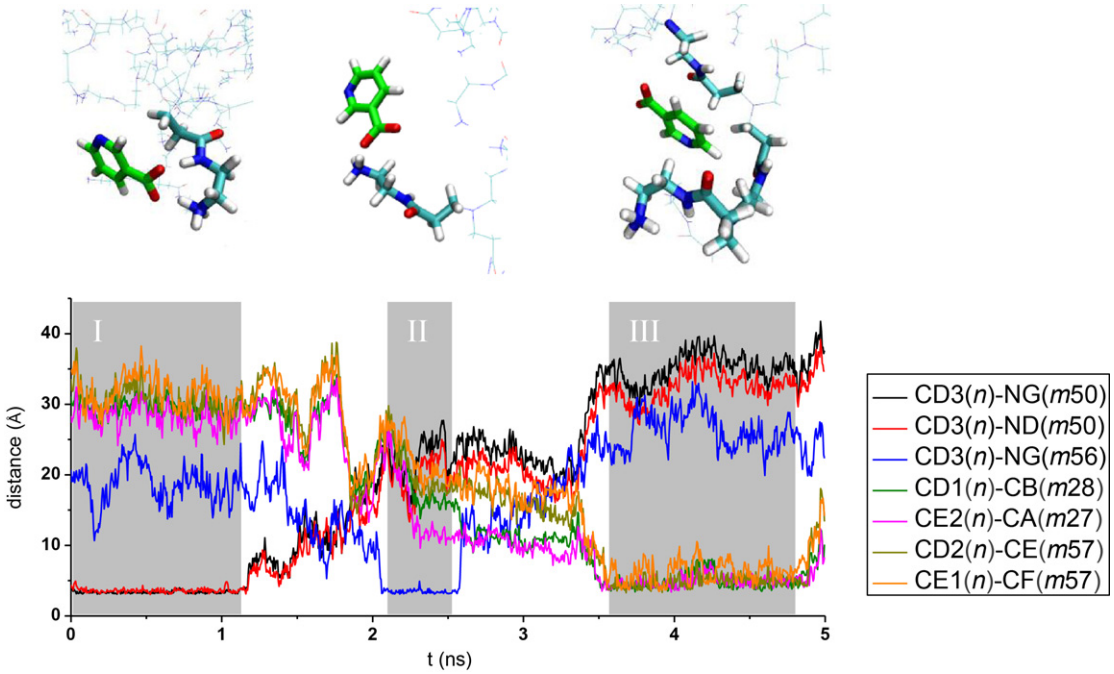

Fig. 5. Distances between nicotinate and PAMAM-G3 atoms extracted from 5-ns MD simulations using the initial structures of Fig. 3A (MD-A). Sites where strong interactions between nicotinate and PAMAM-G3 took place during MD simulation are represented by gray areas and roman numerals; snapshots of the structures in these sites are shown at the top of the figure.

between carbon CE1 of nicotinate and carbon CF of *m*57 (distances CD1(*n*)–CB(*m*28), CE2(*n*)–CA(*m*27), CD2(*n*)–CE(*m*57), and CE1(*n*)–CF(*m*57), respectively in Fig. 5), had values below 10 Å. This VdW interaction was also broken before arriving to the end of the simulation.

During the MD-A, nicotinate maintained its closeness to PAMAM surface. It broke out in some occasions HB or VdW interactions with PAMAM, but it was attracted by the dendrimer surface again. To visualize a distribution of the electrostatic potential (EP) in MD-A, internal electrostatic potentials were computed by using 'pmepot' plugin of VMD [42]. To determine the mean EP, instantaneous electrostatic potentials were averaged over the entire MD-A trajectory. Fig. 6 shows the field lines describing the three-dimensional (3D) EP in our simulation. The field lines change from negatively biased regions in the solvent to positively biased regions near the surface amines. According to the superposition of the EP map and positions of the above mentioned sites I, II and III (Fig. 6), the nicotinate molecule 'jumped' from one positive center to another during the MD-A simulation. This fact means that the dendrimer induces an electric field which attracts the nicotinate molecules. The nicotinate can go to the solvent but it has more stable interactions with the PAMAM surface.

A scheme of the pathway of nicotinate around PAMAM-G3 surface according to 5-ns MD simulation using conformation B as starting point (MD-B) is represented in Fig. 4B; in addition, Fig. 7 shows distances between some atoms of nicotinate and atoms of the monomers that the drug found on its way. First, the nicotinate molecule was near the monomer *m*42 of PAMAM-G3 (site I, Fig. 4B). At this site, an HB between the carboxylate of nicotinate and surface amine of *m*42 was formed. This was deduced from the analysis of the distances between carbon CD3 of nicotinate and nitrogen NG of *m*42 (distance CD3(*n*)–NG(*m*42) in Fig. 7). This distance took values around 3.40 Å from 0.23 to 0.45 ns of the simulation. After this time, nicotinate molecule moved away from the surface of PAMAM and entered into the solvent. At 1.15 ns, nicotinate approximated to the monomer *m*40 of PAMAM-G3 (site II, Fig. 4B). From this time to the end of the simulation, the distances between carbon CD3 of nicotinate and nitrogen atoms NG and ND of *m*40 (distances CD3(*n*)–NG(*m*40) and CD3(*n*)–ND(*m*40) in Fig. 7) took values around 3.38 and 3.65 Å respectively due to HBs formed between the carboxylate of nicotinate and amine and amide N atoms of *m*40. After 1.59 ns, additional interactions between pyridine ring of nicotinate and methylene groups of inner monomers *m*17 and *m*18 were formed. From this time to the end of the simulation MD-B, the distance between carbon CD1 of nicotinate and carbon CE of *m*18, and the distance between carbon CE2 of nicotinate and carbon CB of *m*17 (distances CD1(*n*)–CE(*m*18) and CE2(*n*)–CB(*m*17) respectively in Fig. 7), took values below 9 Å. Since the interactions at site II existed for more than 3 ns in MD-B, we can conclude that the drug and dendrimer interact in a stable complex when both electrostatic and hydrophobic interactions exist together.

The third 5-ns MD simulation (MD-C) was carried out from a structure C where electrostatic and VdW interactions between nicotinate and PAMAM-G3 monomer are both present from the start. The scheme of the pathway of nicotinate around PAMAM-G3 surface during MD-C (simulation using conformation C as starting point), represented in Fig. 4C, shows that the drug interacted only with monomers *m*30 and *m*13 at site denoted as I. Fig. 8 shows that distances between carbon CD3 of nicotinate and nitrogen atoms NG and ND of *m*30 (distances CD3(*n*)–NG(*m*30) and CD3(*n*)–ND(*m*30) in Fig. 8) took values around 3.37 and 3.67 Å respectively during all the simulation. In addition, the distance between carbon CD2 of nicotinate and carbon CE of *m*13, and the distance between carbon CE2 of nicotinate and carbon CF of *m*13 (distances CD2(*n*)–CE(*m*13) and CE2(*n*)–CF(*m*13) respectively in Fig. 8) took values below 9 Å. The simulation MD-C corroborates the above mentioned conclusion about the existence of a stable complex of the drug and dendrimer where electrostatic and VdW interactions are formed at the same time.

Our work allows analyzing the origin of the physicochemical properties that govern the dendrimer–drug affinity. The electrostatic interactions between the amino terminal and amide groups of the dendrimer surface and the carboxyl group of NA seem a principal component of this type of interaction. However, we found

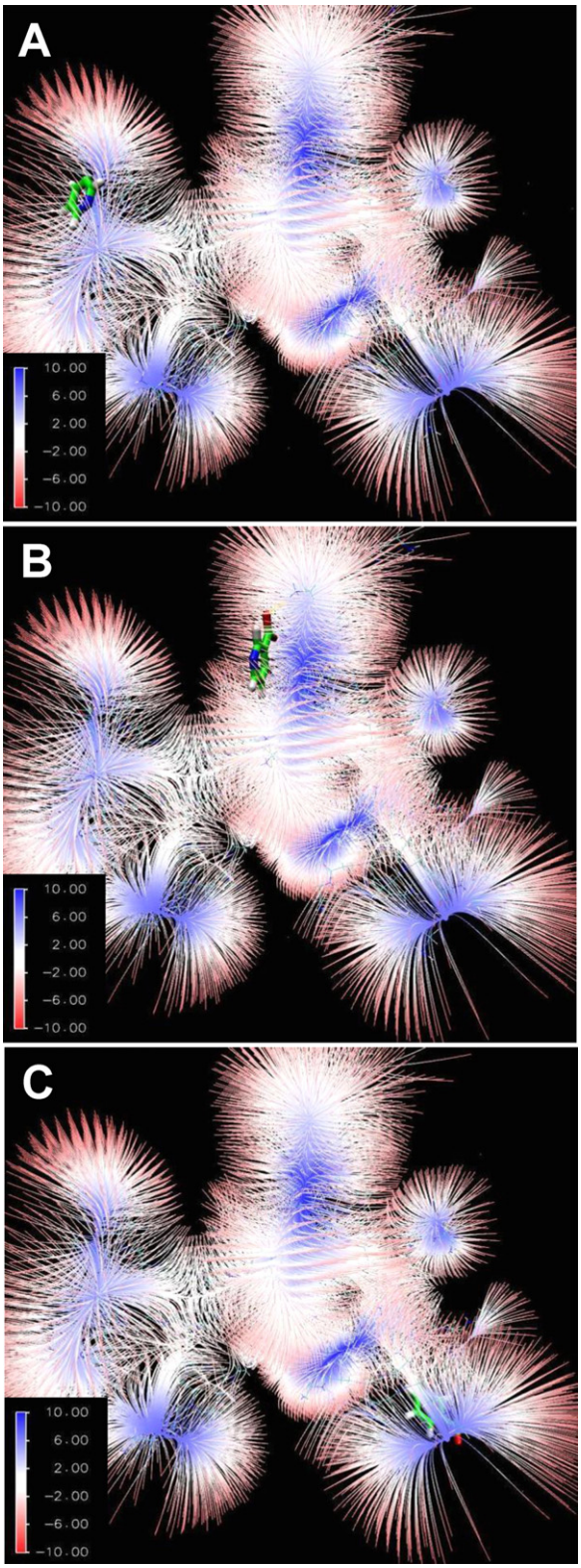

Fig. 6. Electrostatic potential 3D map of PAMAM-G3 during 5-ns simulation using conformation A as starting point (MD-A) with (A) a snapshot of the nicotinate at site I, (B) a snapshot of the nicotinate at site II, and (C) a snapshot of the nicotinate at site III.

that the interaction of the drug with the hydrophobic groups is also important. These results are in agreement with our previous results where the relative affinity of nonsteroidal anti-inflammatory drugs (NSAIDs) by PAMAM is controlled, largely, by the interaction

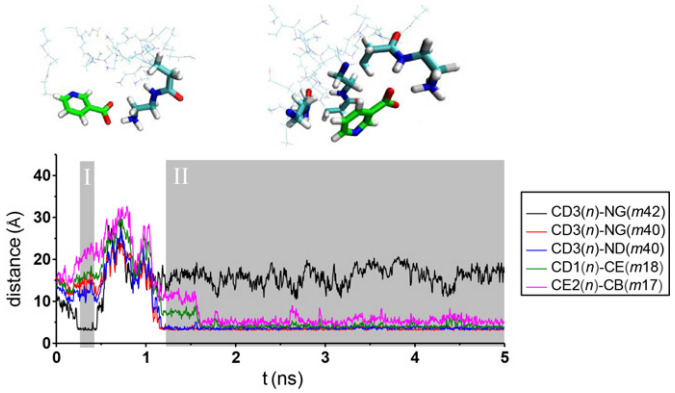

Fig. 7. Distances between nicotinate and PAMAM-G3 atoms extracted from 5-ns MD simulations using the initial structures of Fig. 3B (MD-B). Sites where strong interactions between nicotinate and PAMAM-G3 took place during MD simulation are represented by gray areas and roman numerals; snapshots of the structures in these sites are shown at the top of the figure.

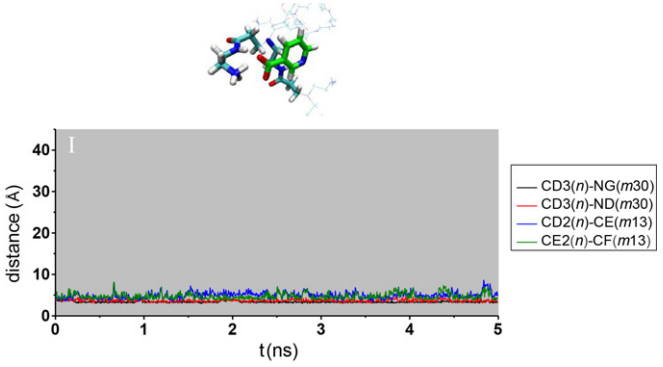

Fig. 8. Distances between nicotinate and PAMAM-G3 atoms extracted from 5-ns MD simulations using the initial structures of Fig. 3C (MD-C). Sites where strong interactions between nicotinate and PAMAM-G3 took place during MD simulation are represented by gray areas and roman numerals; snapshots of the structures in these sites are shown at the top of the figure.

of the drug with the hydrophobic cavities of the dendrimer [43].

4. Conclusions

Dendrimers serve as macromolecular hosts. The host–guest binding can either take place in the cavities of the dendrimer core, or at the multivalent surface or outer shell of the dendrimer. Some experiments suggest that the interactions between the host and the guest molecule can be specific [44]; they can be governed by the molecular size of the guest molecule, the physical size of the cavities in the host, and the specific chemical interactions. The knowledge of these geometrical and chemical features could lead to planning a modification of the dendrimer yielding a host molecule with new desired properties.

In this work, the interactions between PAMAM-G3 and nicotinic acid (NA) were studied by using MD simulations. The following conclusions have been drawn from this study:

1. PAMAM-G3 with internal tertiary amine groups unprotonated (at pH 6) provides a favorable environment for NA inclusion. However, when internal tertiary amine groups are protonated (at pH 3), the PAMAM cavities are less hydrophobic and drug–dendrimer interactions become similar to drug–solvent interactions.

2. NA prefers to interact with surface groups of PAMAM-G3, instead of to be encapsulated in the macromolecule interior.
3. At pH 6, PAMAM-G3 induces an electric field which attracts the NA molecules.
4. PAMAM-G3 and NA form a stable complex in the surface of the dendrimer when electrostatic and VdW interactions between the drug and the monomers are formed at the same time.

References

[1] H.-J. Schneider, Binding mechanisms in supramolecular complexes, Angewandte Chemie International Edition 48 (2009) 3924–3977.
[2] R. Villalonga, R. Cao, A. Fragoso, A.E. Damiao, P.D. Ortiz, J. Caballero, Supramolecular assembly of [beta]-cyclodextrin-modified gold nanoparticles and Cu, Zn-superoxide dismutase on catalase, Journal of Molecular Catalysis B: Enzymatic 35 (2005) 79–85.
[3] Y. Liu, Z.-L. Yu, Y.-M. Zhang, D.-S. Guo, Y.-P. Liu, Supramolecular architectures of β-cyclodextrin-modified chitosan and pyrene derivatives mediated by carbon nanotubes and their DNA condensation, Journal of the American Chemical Society 130 (2008) 10431–10439.
[4] S. Svenson, Dendrimers as versatile platform in drug delivery applications, European Journal of Pharmaceutics and Biopharmaceutics 71 (2009) 445–462.
[5] T. Dutta, N.K. Jain, N.A.J. McMillan, H.S. Parekh, Dendrimer nanocarriers as versatile vectors in gene delivery, Nanomedicine 6 (2010) 25–34.
[6] S.-C. Lo, P.L. Burn, Development of dendrimers: macromolecules for use in organic light-emitting diodes and solar cells, Chemical Reviews 107 (2007) 1097–1116.
[7] T. Barrett, G. Ravizzini, P. Choyke, H. Kobayashi, Dendrimers in medical nanotechnology, IEEE Engineering in Medicine and Biology Magazine 28 (2009) 12–22.
[8] W.-D. Jang, K.M. Kamruzzaman Selim, C.-H. Lee, I.-K. Kang, Bioinspired application of dendrimers: from bio-mimicry to biomedical applications, Progress in Polymer Science 34 (2009) 1–23.
[9] D.A. Tomalia, H. Baker, J. Dewald, M. Hall, G. Kallos, S. Martin, et al., A new class of polymers: starburst-dendritic macromolecules, Polymer Journal 17 (1985) 117–132.
[10] D.A. Tomalia, A.M. Naylor, W.A. Goddard, Starburst dendrimers: molecular-level control of size, shape, surface chemistry, topology, and flexibility from atoms to macroscopic matter, Angewandte Chemie International Edition 29 (1990) 138–175.
[11] I. Lee, B.D. Athey, A.W. Wetzel, W. Meixner, J.R. Baker, Structural molecular dynamics studies on polyamidoamine dendrimers for a therapeutic application: effects of ph and generation, Macromolecules 35 (2002) 4510–4520.
[12] C. Yiyun, X. Tongwen, Solubility of nicotinic acid in polyamidoamine dendrimer solutions, European Journal of Medical Chemistry 40 (2005) 1384–1389.
[13] W. Yang, Y. Li, Y. Cheng, Q. Wu, L. Wen, T. Xu, Evaluation of phenylbutazone and poly(amidoamine) dendrimers interactions by a combination of solubility, 2D-NOESY NMR, and isothermal titration calorimetry studies, Journal of Pharmaceutical Sciences 98 (2009) 1075–1085.
[14] J. Hu, Y. Cheng, Y. Ma, Q. Wu, T. Xu, Host–guest chemistry and physicochemical properties of the dendrimer–mycophenolic acid complex, Journal of Physical Chemistry B 113 (2009) 64–74.
[15] Y. Cheng, Y. Li, Q. Wu, J. Zhang, T. Xu, Generation-dependent encapsulation/electrostatic attachment of phenobarbital molecules by poly(amidoamine) dendrimers: evidence from 2D-NOESY investigations, European Journal of Medical Chemistry 44 (2009) 2219–2223.
[16] K.N. Green, J.S. Steffan, H. Martinez-Coria, X. Sun, S.S. Schreiber, L.M. Thompson, et al., Nicotinamide restores cognition in Alzheimer's disease transgenic mice via a mechanism involving sirtuin inhibition and selective reduction of Thr231-Phosphotau, Journal of Neuroscience 28 (2008) 11500–11510.
[17] T.A. Ban, Nicotinic acid in the treatment of schizophrenias, Neuropsychobiology 1 (1975) 133–145.
[18] C.A. Appleby, B.A. Wittenberg, J.B. Wittenberg, Nicotinic acid as a ligand affecting leghemoglobin structure and oxygen reactivity, Proceedings of the National Academy of Sciences of the United States of America 70 (1973) 564–568.
[19] E. Darve, A. Pohorille, Calculating free energies using average force, Journal of Chemical Physics 115 (2001) 9169–9183.
[20] E. Darve, D. Rodriguez-Gomez, A. Pohorille, Adaptive biasing force method for scalar and vector free energy calculations, Journal of Chemical Physics 128 (2008) 144120.
[21] Hyperchem 7.0, Hypercube, Inc., Gainesville, FL, USA, 2002.
[22] M.J.S. Dewar, E.G. Zoebisch, E.F. Healy, J.J.P. Stewart, Development and use of quantum mechanical molecular models. 76. AM1: a new general purpose quantum mechanical molecular model, Journal of the American Chemical Society 107 (1985) 3902–3909.
[23] A.D. MacKerell, D. Bashford, M. Bellott, R.L. Dunbrack, J.D. Evanseck, M.J. Field, et al., All-atom empirical potential for molecular modeling and dynamics studies of proteins, Journal of Physical Chemistry B 102 (1998) 3586–3616.
[24] D. Yin, Parametrization for Empirical Force Field Calculations & A Theoretical Study of Membrane Permeability of Pyridine Derivatives, University of Maryland, 1997 http://stuff.mit.edu:8001/afs/athena/software/vmd_v1.8.7/distrib/vmd-1.8.7/plugins/noarch/tcl/trunctraj1.5/toppar/stream/toppar_all22_prot_pyridines.str
[25] W. Humphrey, A. Dalke, K. Schulten, VMD: visual molecular dynamics, Journal of Molecular Graphics 14 (1996) 33–38.
[26] D. Cakara, J. Kleimann, M. Borkovec, Microscopic protonation equilibria of poly(amidoamine) dendrimers from macroscopic titrations, Macromolecules 36 (2003) 4201–4207.
[27] J.C. Phillips, R. Braun, W. Wang, J. Gumbart, E. Tajkhorshid, E. Villa, et al., Scalable molecular dynamics with NAMD, Journal of Computational Chemistry 26 (2005) 1781–1802.
[28] W.L. Jorgensen, J. Chandrasekhar, J.D. Madura, R.W. Impey, M.L. Klein, Comparison of simple potential functions for simulating liquid water, Journal of Chemical Physics 79 (1983) 926–935.
[29] Y. Liu, V.S. Bryantsev, M.S. Diallo, W.A. Goddard III, PAMAM dendrimers undergo pH responsive conformational changes without swelling, Journal of the American Chemical Society 131 (2009) 2798–2799.
[30] L. Porcar, Y. Liu, R. Verduzco, K. Hong, P.D. Butler, L.J. Magid, et al., Structural investigation of PAMAM dendrimers in aqueous solutions using small-angle neutron scattering: effect of generation, Journal of Physical Chemistry B 112 (2008) 14772–14778.
[31] T.J. Prosa, B.J. Bauer, E.J. Amis, D.A. Tomalia, R. Scherrenberg, A SAXS study of the internal structure of dendritic polymer systems, Journal of Polymer Science Part B: Polymer Physics 35 (1997) 2913–2924.
[32] P.K. Maiti, T. Cagın, G. Wang, W.A. Goddard, Structure of PAMAM dendrimers: generations 1 through 11, Macromolecules 37 (2004) 6236–6254.
[33] G.M. Pavan, L. Albertazzi, A. Danani, Ability to adapt: different generations of PAMAM dendrimers show different behaviors in binding siRNA, Journal of Physical Chemistry B 114 (2010) 2667–2675.
[34] G.M. Pavan, P. Posocco, A. Tagliabue, M. Maly, A. Malek, A. Danani, et al., PAMAM dendrimers for siRNA delivery: computational and experimental insights, Chemistry – A European Journal 16 (2010) 7781–7795.
[35] L.B. Jensen, G.M. Pavan, M.R. Kasimova, S. Rutherford, A. Danani, H.M. Nielsen, et al., Elucidating the molecular mechanism of PAMAM–siRNA dendriplex self-assembly: effect of dendrimer charge density, International Journal of Pharmaceutics 416 (2011) 410–418.
[36] G. Pistolis, A. Malliaris, D. Tsiourvas, C.M. Paleos, Poly(propyleneimine) dendrimers as pH-sensitive controlled-release systems, Chemistry – A European Journal 5 (1999) 1440–1444.
[37] J. Hénin, E. Tajkhorshid, K. Schulten, C. Chipot, Diffusion of glycerol through *Escherichia coli* aquaglyceroporin GlpF, Biophysical Journal 94 (2008) 832–839.
[38] F. Dehez, E. Pebay-Peyroula, C. Chipot, Binding of ADP in the mitochondrial ADP/ATP carrier is driven by an electrostatic funnel, Journal of the American Chemical Society 130 (2008) 12725–12733.
[39] G. Lamoureux, M.L. Klein, S. Bernèche, A stable water chain in the hydrophobic pore of the AmtB ammonium transporter, Biophysical Journal 92 (2007) L82–L84.
[40] W. Cai, T. Sun, P. Liu, C. Chipot, X. Shao, Inclusion mechanism of steroid drugs into β-cyclodextrins. Insights from free energy calculations, Journal of Physical Chemistry B 113 (2009) 7836–7843.
[41] J. Lim, G.M. Pavan, O. Annunziata, E.E. Simanek, Experimental and computational evidence for an inversion in guest capacity in high-generation triazine dendrimer hosts, Journal of the American Chemical Society 134 (2012) 1942–1945.
[42] A. Aksimentiev, K. Schulten, Imaging α-hemolysin with molecular dynamics: ionic conductance, osmotic permeability, and the electrostatic potential map, Biophysical Journal 88 (2005) 3745–3761.
[43] F. Avila-Salas, C. Sandoval, J. Caballero, S. Guiñez-Molinos, L.S. Santos, R.E. Cachau, et al., Study of interaction energies between the PAMAM dendrimer and nonsteroidal anti-inflammatory drug using a distributed computational strategy and experimental analysis by ESI-MS/MS, Journal of Physical Chemistry B 116 (2012) 2031–2039.
[44] C. Yiyun, X. Tongwen, Dendrimers as potential drug carriers. Part I. Solubilization of non-steroidal anti-inflammatory drugs in the presence of polyamidoamine dendrimers, European Journal of Medical Chemistry 40 (2005) 1188–1192.